



## Catabolic and anabolic energy for chemolithoautotrophs in deep-sea hydrothermal systems hosted in different rock types

Jan P. Amend<sup>a,\*</sup>, Thomas M. McCollom<sup>b</sup>, Michael Hentscher<sup>c</sup>, Wolfgang Bach<sup>c</sup>

<sup>a</sup> Department of Earth Sciences and Department of Biological Sciences, University of Southern California, Los Angeles, CA 90089-0740, USA

<sup>b</sup> Laboratory of Atmospheric and Space Physics, University of Colorado, Boulder, CO 80309, USA

<sup>c</sup> Department of Geosciences, University of Bremen, 28334 Bremen, Germany

Received 8 February 2011; accepted in revised form 11 July 2011; available online 2 August 2011

### Abstract

Active deep-sea hydrothermal vents are hosted by a range of different rock types, including basalt, peridotite, and felsic rocks. The associated hydrothermal fluids exhibit substantial chemical variability, which is largely attributable to compositional differences among the underlying host rocks. Numerical models were used to evaluate the energetics of seven inorganic redox reactions (potential catabolisms of chemolithoautotrophs) and numerous biomolecule synthesis reactions (anabolism) in a representative sampling of these systems, where chemical gradients are established by mixing hydrothermal fluid with seawater. The wide ranging fluid compositions dictate demonstrable differences in Gibbs energies ( $\Delta G_r$ ) of these catabolic and anabolic reactions in three peridotite-hosted, six basalt-hosted, one troctolite-basalt hybrid, and two felsic rock-hosted systems. In peridotite-hosted systems at low to moderate temperatures ( $< \sim 45$  °C) and high seawater:hydrothermal fluid (SW:HF) mixing ratios ( $> 10$ ), hydrogen oxidation yields the most catabolic energy, but the oxidation of methane, ferrous iron, and sulfide can also be moderately exergonic. At higher temperatures, and consequent SW:HF mixing ratios  $< 10$ , anaerobic processes dominate the energy landscape; sulfate reduction and methanogenesis are more exergonic than any of the aerobic respiration reactions. By comparison, in the basalt-hosted and felsic rock-hosted systems, sulfide oxidation was the predominant catabolic energy source at all temperatures (and SW:HF ratios) considered. The energetics of catabolism at the troctolite-basalt hybrid system were intermediate to these extremes. Reaction energetics for anabolism in chemolithoautotrophs—represented here by the synthesis of amino acids, nucleotides, fatty acids, saccharides, and amines—were generally most favorable at moderate temperatures (22–32 °C) and corresponding SW:HF mixing ratios ( $\sim 15$ ). In peridotite-hosted and the troctolite-basalt hybrid systems,  $\Delta G_r$  for primary biomass synthesis yielded up to  $\sim 900$  J per g dry cell mass. The energetics of anabolism in basalt- and felsic rock-hosted systems were far less favorable. The results suggest that in peridotite-hosted (and troctolite-basalt hybrid) systems, compared with their basalt (and felsic rock) counterparts, microbial catabolic strategies—and consequently variations in microbial phylotypes—may be far more diverse and some biomass synthesis may yield energy rather than imposing a high energetic cost.

© 2011 Elsevier Ltd. All rights reserved.

### 1. INTRODUCTION

Microbiological activity in deep-sea sediments has received considerable attention in recent years (Jørgensen and D'Hondt, 2006; Biddle et al., 2008; Roussel et al.,

2008; D'Hondt et al., 2009; Webster et al., 2009). Populations there can be large, especially along continental margins (Parkes et al., 2000), but cellular processes are generally linked to the limited input of photosynthetically derived nutrients from the overlying water column (Jahnke, 1996; D'Hondt et al., 2004). In the extremely low productivity South Pacific Gyre—and by inference, in other oligotrophic open ocean regions—organic matter influx to the

\* Corresponding author.

E-mail address: [jan.amend@usc.edu](mailto:jan.amend@usc.edu) (J.P. Amend).

sediments is very low, and radiolytic  $H_2$  may be a significant electron donor for the very dilute and very low activity resident subsurface microbial communities (D'Hondt et al., 2009). In contrast, deep-sea hydrothermal systems, where hot, chemically reduced vent fluids mix with cold, oxidized seawater, provide chemical energy to stimulate robust microbial activity and *in situ* biomass production (McCollom, 2007). More than 150 distinct active hydrothermal vents have now been identified along the ~60,000 km-long ocean ridge system and in back-arc basins (Hannington et al., 2005). In mixing regimes at these sites, seawater is the main source of inorganic carbon for anabolic (biomass synthesis) processes and of oxidants for catabolic (ATP generating) processes; vent fluids provide the reductants for both anabolic and catabolic processes.

Different thermodynamic models have been used to quantify the *in situ* energetics of microbial metabolism in such hydrothermal mixing environments. For example, using a batch mixing approach to study the basalt-hosted hydrothermal system at 21°N on the East Pacific Rise (EPR), it was demonstrated that aerobic respiration at low temperatures (<~40 °C) and anaerobic respiration—especially sulfate reduction and methanogenesis—at elevated temperatures yielded the most energy (McCullom and Shock, 1997; Shock and Holland, 2004). Tivey (2004) expanded on the modeling by considering the effects of diffusive and advective transport on the temperature, chemical composition, and redox reaction energetics in the mixing zones of two basalt-hosted hydrothermal systems, at 21°N on the EPR and the Grotto vent on the Juan de Fuca Ridge. Although pH and porewater oxidation states differed markedly depending on the mixing scenario adopted, the resulting reaction energetics for sulfate reduction, sulfide oxidation, methanogenesis, and methanotrophy were similar in the batch mixing and diffusion/advection models.

In recent years, ultramafic rock-hosted hydrothermal systems have garnered much attention, largely because they generate vent fluids highly enriched in hydrogen and low molecular weight hydrocarbons (Kelley et al., 2001, 2005; Charlou et al., 2002), they are central to several origin of life scenarios (Russell and Hall, 1997; Martin et al., 2008), and they appear to be more widespread than initially surmised (Bach et al., 2002; Früh-Green et al., 2004). Using a batch mixing model, thermodynamic calculations for the Rainbow hydrothermal system on the Mid-Atlantic ridge showed that ultramafic-hosted systems can yield double the catabolic energy of analogous basalt-hosted systems (McCullom, 2007). A batch-mixing approach was also employed to evaluate energy yields from several inorganic redox reactions at several hydrothermal systems (Takai and Nakamura, 2010). Results were reported for two temperatures—“low”, representing 2–50 °C and “high”, representing 50–125 °C.

Complementing the energy modeling of inorganic redox reaction, several studies have evaluated the *in situ* thermodynamics of organic synthesis in hydrothermal systems. In the mixing zone at EPR 21°N, the formation from inorganic starting materials of short-chain carboxylic acids (Shock and Schulte, 1998) and 11 of the 20 protein-forming amino acids (Amend and Shock, 1998) was shown to be exergonic. However, these results represent only a snapshot

of one fluid composition at one hydrothermal vent emanating from one rock type (basalt). Several recent studies focused on organic synthesis (hydrocarbons, organic acids, nucleic acid bases, pentoses) at a wider range of hydrothermal conditions, including systems hosted in ultramafic rocks (Foustoukos and Seyfried, 2004; LaRowe and Regnier, 2008; Proskurowski et al., 2008; Konn et al., 2009; Shock and Canovas, 2010). These studies are also consistent with several origin of life theories that rely on naturally occurring, omnipresent geochemical energy sources (Baross and Hoffman, 1985; Pace, 1991; Shock et al., 2000; Russell et al., 2005; Martin et al., 2008).

In the present communication, we expanded far beyond previous models to assess the quantitative energy landscape for catabolic and anabolic reactions in 12 hydrothermal systems from four different rock types: three are peridotite-hosted (Rainbow, Logatchev, Lost City), six are basalt-hosted (Edmond, Endeavor, EPR 21°N, Lucky Strike, TAG, Menez Gwen), two are felsic rock-hosted (Brothers, Mariner), and one is thought to be a troctolite-basalt hybrid (Kairei); in this hybrid system, fluids issue through basalt, but they show chemical evidence for reactions with troctolites, which are abundant in the Kairei area (Nakamura et al., 2009). Basalt-hosted systems with transient high- $H_2$  gas phases (e.g., A-vent at EPR 9°50'N, (Lilley et al., 2003)) were not included here, because the period of abnormal flux is very short relative to the life-time of the system. Our numerical modeling applies most directly to vent environments where fluid compositions are dominated by mixing. These include, but are not limited to, vent plumes, seafloor settings, and shallow subseafloor zones where mixed solutions of distinct and specific temperatures and chemical compositions are generated.

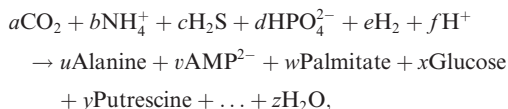
## 2. METHODS

In the first part of this study, seven catabolic reactions were considered (see Table 1); four of them represent aerobic respiration of different inorganic electron donors, and three of them denote anaerobic respiration. In the second part, the energetics of anabolism were evaluated. In this case, biomass was divided into the amino acids, nucleotides, fatty acids, saccharides, and amines that make up the biopolymers (proteins, nucleic acids, membranes, cell walls, and other major cellular components) that constitute a model prokaryotic cell (Morowitz, 1968; McCollom and Amend, 2005; Amend and McCollom, 2009). The composition of *Escherichia coli* was adopted as a representative prokaryotic biomass, positing that differences in cellular make-up among various archaea and bacteria (all of which are amino acid-rich and saccharide-poor like *E. coli*) are secondary relative to compositional differences in the hydrothermal fluids. As detailed biomolecule concentrations become available for a wider range of archaea and bacteria, the consequences of cellular composition differences on anabolism energetics can be readily investigated. The monomer units, their prokaryote cellular concentrations, and the individual synthesis reactions from aqueous inorganic compounds are given in Table 2. The net synthesis reaction for cellular biomass can then be written as:

Table 1  
Inorganic redox reactions.

Aerobic sulfide oxidation	$\text{H}_2\text{S} + 2\text{O}_2 \rightarrow \text{SO}_4^{2-} + 2\text{H}^+$
Aerobic methane oxidation	$\text{CH}_4 + 2\text{O}_2 \rightarrow \text{CO}_2 + 2\text{H}_2\text{O}$
Aerobic iron oxidation	$4\text{Fe}^{2+} + \text{O}_2 + 10\text{H}_2\text{O} \rightarrow 4\text{Fe}(\text{OH})_3 + 8\text{H}^+$
Aerobic hydrogen oxidation	$2\text{H}_2 + \text{O}_2 \rightarrow 2\text{H}_2\text{O}$
Hydrogenotrophic sulfate reduction	$4\text{H}_2 + \text{SO}_4^{2-} + 2\text{H}^+ \rightarrow \text{H}_2\text{S} + 4\text{H}_2\text{O}$
Hydrogenotrophic methanogenesis	$4\text{H}_2 + \text{CO}_2 \rightarrow \text{CH}_4 + 2\text{H}_2\text{O}$
Anaerobic oxidation of methane (AOM)	$\text{CH}_4 + \text{SO}_4^{2-} + 2\text{H}^+ \rightarrow \text{CO}_2 + \text{H}_2\text{S} + 2\text{H}_2\text{O}$

All compounds are in the aqueous phase, except  $\text{Fe}(\text{OH})_3$  which represents the mineral ferrihydrite.



where the reaction products represent the aforementioned monomer building blocks.

The compositions of the mixed hydrothermal solutions were calculated from those of the end-member vent fluids and seawater (Table 3) using the REACT module in the computer code Geochemist's Workbench™. The reaction path mimics the incremental titration of small aliquots of hot vent fluid into cold seawater, reevaluating the chemical speciation of the mixed solution at each step. Minerals were not allowed to precipitate during mixing. Note that permitting mineral precipitation would slightly lower the amounts of energy in the iron and sulfide oxidation reactions. However, as previously shown (McCullom, 2000), the redox energy would still be available, but now transferred to reactions involving solid forms of iron and sulfide. As is standard practice, redox reactions were prohibited, while acid–base reactions were allowed to equilibrate. The temperatures of the calculated mixed solutions were taken to scale linearly with the temperatures of the end-members; differences in heat capacities between seawater and vent fluid only lead to minimal deviation from this linear trend.

Values of Gibbs energy ( $\Delta G_r$ ) for the catabolic and anabolic reactions were computed with the relation

$$\Delta G_r = \Delta G_r^\circ + RT \ln Q_r,$$

where  $\Delta G_r^\circ$  denotes the standard Gibbs energy of reaction,  $R$  and  $T$  represent the gas constant and temperature in Kelvin, respectively, and  $Q_r$  stands for the activity product of reaction  $r$ , which is evaluated with the relation

$$Q_r = \prod a_i^{v_{i,r}},$$

where  $a_i$  denotes the activity of species  $i$  raised to the stoichiometric reaction coefficient  $v_{i,r}$ . The  $Q$ -term accounts for the chemical compositions of the mixed hydrothermal solutions and the intracellular concentrations of the biomass building blocks. Values of  $\Delta G_r^\circ$  were calculated at 50 MPa and the temperatures of interest with the computer code SUPCRT92 (Johnson et al., 1992), which relies on the relation

$$\Delta G_r^\circ = \sum v_{i,r} \Delta G_i^\circ,$$

where  $\Delta G_i^\circ$  represents the apparent standard Gibbs energy of formation of the  $i^{\text{th}}$  species in reaction  $r$ . Values of

$\Delta G_i^\circ$  for the aqueous species and minerals used in the catabolic and anabolic reactions were computed with the revised Helgeson–Kirkham–Flowers (HKF) equations of state (Helgeson et al., 1978, 1981; Shock and Helgeson, 1988, 1990; Tanger and Helgeson, 1988; Shock et al., 1989, 1992), with additional internally consistent thermodynamic data from several different regression analyses (Amend and Plyasunov, 2001; Dick et al., 2006; LaRowe and Helgeson, 2006; Amend and McCollom, 2009). We used the B-dot equation for calculations of activity coefficients of dissolved inorganic species with B-dot and extended Debye–Hückel parameters, as well as hard core diameters, from a recent compilation (Wolery, 2004). Dissolved neutral species were assigned an activity coefficient of 1.0, except nonpolar dissolved gases, for which  $\text{CO}_2$  activity coefficients (Drummond, 1981) were used. For all biomolecules, an activity of  $10^{-12}$  was assumed (McCullom and Amend, 2005). The respective differences in values of  $\Delta G_r^\circ$  due to the corresponding differences in pressure between 50 MPa and *in situ* values are relatively minimal. Note also that for all anabolic reactions, the resulting estimates of reaction energetics refer only to the net energetic change between the inorganic precursors and the resulting biomolecule, and do not include the additional energetic costs imposed by the inevitable inefficiencies of biochemical pathways. A discussion on the impact of these inefficiencies on the overall energetic costs of biomass synthesis can be found in McCollom and Amend (2005).

The general calculation procedure is as follows: (1) Speciating the measured hydrothermal fluid composition at 25 °C, using reported pH values at this temperature. (2) Determining the *in situ* pH by ‘heating’ (through modeling) this fluid to the *in situ* temperature, while allowing all acid–base reactions to equilibrate in the computations. (3) Mixing this re-specified fluid with seawater, suppressing redox reactions and allowing acid–base reactions to equilibrate. (This approach is reasonable, because acid–base reactions equilibrate at the time scales of mixing, but redox reactions do not.) (4) Using the activities of relevant species to calculate the Gibbs energies as described above.

The amount of energy available from catabolic reactions as a function of temperature (or, equivalently, mixing ratio) were calculated by multiplying the calculated Gibbs energy for the reaction at each temperature by the concentration of reactants in the mixed fluid, taking into account the stoichiometry of the reaction and the reactant that is present in limiting supply, and then multiplying by the total amount of mixed fluid at that temperature (McCullom and Shock,

Table 2  
Biomass composition and synthesis reactions.

Biomass monomer	Amount <sup>a</sup> (mg/g)	Biomass synthesis reaction
Alanine	48.4	$3\text{CO}_2 + \text{NH}_4^+ + 6\text{H}_2 = \text{C}_3\text{H}_7\text{NO}_2 + 4\text{H}_2\text{O} + \text{H}^+$
Arginine <sup>+</sup>	49.0	$6\text{CO}_2 + 4\text{NH}_4^+ + 11\text{H}_2 = \text{C}_6\text{H}_{15}\text{N}_4\text{O}_2^+ + 10\text{H}_2\text{O} + 3\text{H}^+$
Asparagine	30.3	$4\text{CO}_2 + 2\text{NH}_4^+ + 6\text{H}_2 = \text{C}_4\text{H}_8\text{N}_2\text{O}_3 + 5\text{H}_2\text{O} + 2\text{H}^+$
Aspartate	30.5	$4\text{CO}_2 + \text{NH}_4^+ + 6\text{H}_2 = \text{C}_4\text{H}_6\text{NO}_4^- + 4\text{H}_2\text{O} + 2\text{H}^+$
Cysteine	10.5	$3\text{CO}_2 + \text{NH}_4^+ + \text{H}_2\text{S} + 5\text{H}_2 = \text{C}_3\text{H}_7\text{NO}_2\text{S} + 4\text{H}_2\text{O} + \text{H}^+$
Glutamate	40.8	$5\text{CO}_2 + \text{NH}_4^+ + 9\text{H}_2 = \text{C}_5\text{H}_8\text{NO}_4^- + 6\text{H}_2\text{O} + 2\text{H}^+$
Glutamine	36.5	$5\text{CO}_2 + 2\text{NH}_4^+ + 9\text{H}_2 = \text{C}_5\text{H}_{10}\text{N}_2\text{O}_3 + 7\text{H}_2\text{O} + 2\text{H}^+$
Glycine	43.7	$2\text{CO}_2 + \text{NH}_4^+ + 3\text{H}_2 = \text{C}_2\text{H}_5\text{NO}_2 + 2\text{H}_2\text{O} + \text{H}^+$
Histidine	14.0	$6\text{CO}_2 + 3\text{NH}_4^+ + 10\text{H}_2 = \text{C}_6\text{H}_9\text{N}_3\text{O}_2 + 10\text{H}_2\text{O} + 3\text{H}^+$
Isoleucine	36.2	$6\text{CO}_2 + \text{NH}_4^+ + 15\text{H}_2 = \text{C}_6\text{H}_{13}\text{NO}_2 + 10\text{H}_2\text{O} + \text{H}^+$
Leucine	56.1	$6\text{CO}_2 + \text{NH}_4^+ + 15\text{H}_2 = \text{C}_6\text{H}_{13}\text{NO}_2 + 10\text{H}_2\text{O} + \text{H}^+$
Lysine <sup>+</sup>	47.7	$6\text{CO}_2 + 2\text{NH}_4^+ + 14\text{H}_2 = \text{C}_6\text{H}_{15}\text{N}_2\text{O}_2^+ + 10\text{H}_2\text{O} + \text{H}^+$
Methionine	21.8	$5\text{CO}_2 + \text{NH}_4^+ + \text{H}_2\text{S} + 11\text{H}_2 = \text{C}_5\text{H}_{11}\text{NO}_2\text{S} + 8\text{H}_2\text{O} + \text{H}^+$
Phenylalanine	29.1	$9\text{CO}_2 + \text{NH}_4^+ + 20\text{H}_2 = \text{C}_9\text{H}_{11}\text{NO}_2 + 16\text{H}_2\text{O} + \text{H}^+$
Proline	24.2	$5\text{CO}_2 + \text{NH}_4^+ + 11\text{H}_2 = \text{C}_5\text{H}_9\text{NO}_2 + 8\text{H}_2\text{O} + \text{H}^+$
Serine	21.5	$3\text{CO}_2 + \text{NH}_4^+ + 5\text{H}_2 = \text{C}_3\text{H}_7\text{NO}_3 + 3\text{H}_2\text{O} + \text{H}^+$
Threonine	28.7	$4\text{CO}_2 + \text{NH}_4^+ + 8\text{H}_2 = \text{C}_4\text{H}_9\text{NO}_3 + 5\text{H}_2\text{O} + \text{H}^+$
Tryptophan	11.0	$11\text{CO}_2 + 2\text{NH}_4^+ + 23\text{H}_2 = \text{C}_{11}\text{H}_{12}\text{N}_2\text{O}_2 + 20\text{H}_2\text{O} + 2\text{H}^+$
Tyrosine	23.7	$9\text{CO}_2 + \text{NH}_4^+ + 19\text{H}_2 = \text{C}_9\text{H}_{11}\text{NO}_3 + 15\text{H}_2\text{O} + \text{H}^+$
Valine	47.1	$5\text{CO}_2 + \text{NH}_4^+ + 12\text{H}_2 = \text{C}_5\text{H}_{11}\text{NO}_2 + 8\text{H}_2\text{O} + \text{H}^+$
AMP <sup>2-</sup>	57.3	$10\text{CO}_2 + 5\text{NH}_4^+ + \text{HPO}_4^{2-} + 15\text{H}_2 = \text{C}_{10}\text{H}_{12}\text{N}_5\text{O}_7\text{P}^{2-} + 17\text{H}_2\text{O} + 5\text{H}^+$
GMP <sup>2-</sup>	73.3	$10\text{CO}_2 + 5\text{NH}_4^+ + \text{HPO}_4^{2-} + 14\text{H}_2 = \text{C}_{10}\text{H}_{12}\text{N}_5\text{O}_8\text{P}^{2-} + 16\text{H}_2\text{O} + 5\text{H}^+$
CMP <sup>2-</sup>	45.5	$9\text{CO}_2 + 3\text{NH}_4^+ + \text{HPO}_4^{2-} + 15\text{H}_2 = \text{C}_9\text{H}_{12}\text{N}_3\text{O}_8\text{P}^{2-} + 14\text{H}_2\text{O} + 3\text{H}^+$
UMP <sup>2-</sup>	43.8	$9\text{CO}_2 + 2\text{NH}_4^+ + \text{HPO}_4^{2-} + 15\text{H}_2 = \text{C}_9\text{H}_{11}\text{N}_2\text{O}_9\text{P}^{2-} + 13\text{H}_2\text{O} + 2\text{H}^+$
dAMP <sup>2-</sup>	8.1	$10\text{CO}_2 + 5\text{NH}_4^+ + \text{HPO}_4^{2-} + 16\text{H}_2 = \text{C}_{10}\text{H}_{12}\text{N}_5\text{O}_6\text{P}^{2-} + 18\text{H}_2\text{O} + 5\text{H}^+$
dGMP <sup>2-</sup>	8.8	$10\text{CO}_2 + 5\text{NH}_4^+ + \text{HPO}_4^{2-} + 15\text{H}_2 = \text{C}_{10}\text{H}_{12}\text{N}_5\text{O}_7\text{P}^{2-} + 17\text{H}_2\text{O} + 5\text{H}^+$
dCMP <sup>2-</sup>	8.8	$9\text{CO}_2 + 3\text{NH}_4^+ + \text{HPO}_4^{2-} + 16\text{H}_2 = \text{C}_9\text{H}_{12}\text{N}_3\text{O}_7\text{P}^{2-} + 15\text{H}_2\text{O} + 3\text{H}^+$
dTMP <sup>2-</sup>	7.9	$10\text{CO}_2 + 2\text{NH}_4^+ + \text{HPO}_4^{2-} + 19\text{H}_2 = \text{C}_{10}\text{H}_{13}\text{N}_2\text{O}_8\text{P}^{2-} + 16\text{H}_2\text{O} + 2\text{H}^+$
Palmitate	28.5	$16\text{CO}_2 + 46\text{H}_2 = \text{C}_{16}\text{H}_{31}\text{O}_2^- + 30\text{H}_2\text{O} + \text{H}^+$
Oleate	17.5	$18\text{CO}_2 + 51\text{H}_2 = \text{C}_{18}\text{H}_{33}\text{O}_2^- + 34\text{H}_2\text{O} + \text{H}^+$
Palmitoleate	21.7	$16\text{CO}_2 + 45\text{H}_2 = \text{C}_{16}\text{H}_{29}\text{O}_2^- + 30\text{H}_2\text{O} + \text{H}^+$
Myristate	3.8	$14\text{CO}_2 + 40\text{H}_2 = \text{C}_{14}\text{H}_{27}\text{O}_2^- + 26\text{H}_2\text{O} + \text{H}^+$
$\beta$ -Hydroxymyristate	8.2	$14\text{CO}_2 + 39\text{H}_2 = \text{C}_{14}\text{H}_{27}\text{O}_3^- + 25\text{H}_2\text{O} + \text{H}^+$
Glycerol	15.3	$3\text{CO}_2 + 7\text{H}_2 = \text{C}_3\text{H}_8\text{O}_3 + 3\text{H}_2\text{O}$
Glucose	4.5	$6\text{CO}_2 + 12\text{H}_2 = \text{C}_6\text{H}_{12}\text{O}_6 + 6\text{H}_2\text{O}$
Heptose	5.3	$7\text{CO}_2 + 14\text{H}_2 = \text{C}_7\text{H}_{14}\text{O}_7 + 7\text{H}_2\text{O}$
Galactose	1.5	$6\text{CO}_2 + 12\text{H}_2 = \text{C}_6\text{H}_{12}\text{O}_6 + 6\text{H}_2\text{O}$
Rhamnose	1.4	$6\text{CO}_2 + 13\text{H}_2 = \text{C}_6\text{H}_{12}\text{O}_5 + 7\text{H}_2\text{O}$
Glucoseamine	3.0	$6\text{CO}_2 + \text{NH}_4^+ + 12\text{H}_2 = \text{C}_6\text{H}_{13}\text{NO}_5 + 7\text{H}_2\text{O} + \text{H}^+$
<i>N</i> -Acetylglucoseamine	8.0	$8\text{CO}_2 + \text{NH}_4^+ + 16\text{H}_2 = \text{C}_8\text{H}_{15}\text{NO}_6 + 10\text{H}_2\text{O} + \text{H}^+$
<i>N</i> -Acetylmuramic acid	8.1	$11\text{CO}_2 + \text{NH}_4^+ + 22\text{H}_2 = \text{C}_{11}\text{H}_{19}\text{NO}_8 + 14\text{H}_2\text{O} + \text{H}^+$
Ethanolamine	8.0	$2\text{CO}_2 + \text{NH}_4^+ + 5\text{H}_2 = \text{C}_2\text{H}_7\text{NO} + 3\text{H}_2\text{O} + \text{H}^+$
Diaminopimelic acid	5.3	$7\text{CO}_2 + 2\text{NH}_4^+ + 14\text{H}_2 = \text{C}_7\text{H}_{14}\text{N}_2\text{O}_4 + 10\text{H}_2\text{O} + 2\text{H}^+$
Putrescine	3.0	$4\text{CO}_2 + 2\text{NH}_4^+ + 11\text{H}_2 = \text{C}_4\text{H}_{12}\text{N}_2 + 8\text{H}_2\text{O} + 2\text{H}^+$
Spermidine	1.0	$7\text{CO}_2 + 3\text{NH}_4^+ + 19\text{H}_2 = \text{C}_7\text{H}_{19}\text{N}_3 + 14\text{H}_2\text{O} + 3\text{H}^+$

<sup>a</sup> Amount of each monomer per g dry weight of cells, based on the composition of *Escherichia coli* given by (Battley, 1991).

1997; McCollom, 2007). The first step in this calculation yields the available energy per kg mixed fluid, while the second yields the energy available per kg of pure hydrothermal vent fluid.

### 3. GEOLOGIC SETTING

The 12 deep-sea hydrothermal systems considered in this study are hosted in four different rock types and are geographically distributed across the three major oceans (Fig. 1). An overview of the geologic settings and principal

characteristics of venting in these hydrothermal areas are given in Table 4.

#### 3.1. Peridotite-hosted systems

Three sites are hosted in mantle peridotite—Rainbow, Logatchev, and Lost City. Rainbow and Logatchev are high-temperature (350–365 °C) black smoker deposits with high concentrations of metals (e.g., 2–24 mM Fe), H<sub>2</sub> (12–19 mM), and CH<sub>4</sub> (>2 mM) (Charlou et al., 2002; Schmidt et al., 2007). Rainbow is located near a nontrans-

Table 3  
Chemical composition of vent fluids and seawater used in this study.

Vent Site	Rock type	T (°C)	pH	Na <sup>+</sup>	Ca <sup>2+</sup>	K <sup>+</sup>	Fe <sup>2+</sup>	Cl <sup>-</sup>	SiO <sub>2</sub>	CH <sub>4</sub>	H <sub>2</sub> S	H <sub>2</sub>	ΣCO <sub>2</sub>	NH <sub>4</sub> <sup>+</sup>	Refs.
Rainbow	P	365	2.8	553	66.6	20.4	24.05	750	6.9	2.5	1.2	16	16	0.1	1–3
Logatchev	P	350	3.3	438	28	22	2.5	515	8.2	2.1	0.65	12	10.1	0.1	1,2
Lost City	P	140	9	607	20	10	ND	650	0.01	2	0.1	16	0.01	0.1	4,5
Kairei	T/B	365	3.44	528	31.3	15.2	6.01	620	16.7	0.17	3.93	7.89	4.76	17.1	6
Edmond	B	382	3.13	721	63.4	44.2	13.9	927	20.8	0.29	4.81	0.14	7.19	39.6	6
Endeavor	B	347	4	352	33	24.6	0.9	426	14	1.6	7.4	0.33	53	503	7,8
EPR 21°N	B	350	4.3	432	15.6	23.2	1.66	490	17.6	0.07	7.3	1.7	5.72	0.1	9–11
Lucky Strike	B	320	3.65	390	35.6	23.4	0.31	465	14.4	0.52	2.7	0.21	24.2	0.1	12
TAG	B	360	3.1	584	26	18	1.64	659	22	0.12	3.5	0.26	3.1	0.1	1,3,13
Menez Gwen	B	280	4.2	315	31.6	22.9	0.03	374	10	1.4	1.6	0.04	21.7	0.1	1,12
Brothers	F	290	2.8	369	33.7	48.8	4.2	502	12.4	6.8	7.86	0.02	35.5	8.88	14,15
Mariner	F	279	2.66	387	40.6	26.4	11.1	531	15.6	7.8	9.7	0.04	69.6	0.1	15
Seawater		2	7.8	441	10.7	9.8	0.00	550	0.13				0.0	1,16	

All concentrations are millimolar (mM), except CH<sub>4</sub> at Brothers and Mariner and NH<sub>4</sub><sup>+</sup> at all sites, which are micromolar (μM). Values of pH are for 25 °C. Rock types are peridotite (P), troctolite-basalt hybrid (T/B), basalt (B), and felsic (F). Seawater composition also includes 27.9 mM SO<sub>4</sub><sup>2-</sup>, 0.2 mM O<sub>2</sub>, and 2.2 mM CO<sub>2</sub> (Charlou et al., 2002). ND denotes ‘not determined’. References are 1: (Charlou et al., 1998), 2: (Charlou et al., 2002), 3: (Douville et al., 2002), 4: (Kelley et al., 2005), 5: (Proskurowski et al., 2006), 6: (Gallant and Von Damm, 2006), 7: (Seewald et al., 2003), 8: (Seyfried et al., 2003), 9: (Von Damm, 1990), 10: (Von Damm et al., 1985), 11: (Welhan and Craig, 1983), 12: (Charlou et al., 2000), 13: (Charlou et al., 1996), 14: (Takai et al., 2009), 15: (Takai et al., 2008), 16: (McCollom, 2007).

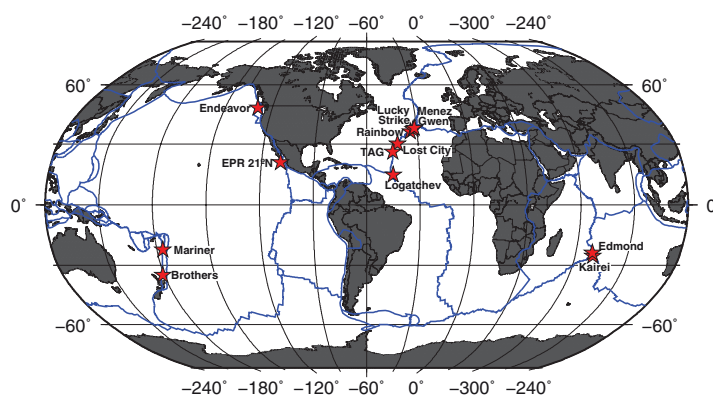


Fig. 1. Tectonic setting of the 12 deep-sea hydrothermal systems considered in the numerical modeling.

form discontinuity and bound to normal faults; Logatchev is situated 7 km east of the rift valley floor on the slope of a detachment fault (German and Parson, 1998; Schroeder et al., 2007). At both locations, mantle peridotite is the principle host lithology, but gabbroic rocks and sparse basalt are also observed in the vicinity of the vent sites (Marques et al., 2006; Petersen et al., 2009). Venting at Rainbow takes place through several groups of extremely active and large black smokers. At Logatchev on the other hand, smoking craters with or without small, fragile sulfide chimneys at the crater rim are typical. The third site—Lost City—is hosted in a diverse suite of mafic and ultramafic rocks that crop out on the cliffs immediately below the edge of the scarp marking the southern termination of the Atlantis Massif (Kelley et al., 2001; Früh-Green et al., 2003; Boschi et al., 2006; Delacour et al., 2008). Alkaline fluids (pH 9–11) vent at temperatures up to 90 °C through carbonate-brucite chimneys that are up to 60 m tall (Kelley and Früh-Green, 2001; Kelley et al., 2005). Hydrogen and

methane concentrations are elevated relative to seawater (1–2 mM CH<sub>4</sub> and up to 16 mM H<sub>2</sub> (Kelley et al., 2005; Proskurowski et al., 2006). Lost City fluids also show evidence for abiogenic production of several low molecular weight organic molecules, including ethane, propane, formate, and acetate (Proskurowski et al., 2008; Lang et al., 2010). Although the fluid temperature at Lost City is lower than that at Rainbow and Logatchev, high H<sub>2</sub> concentrations are typical at all peridotite-hosted systems.

### 3.2. Basalt-hosted systems

Six sites considered here occur in basalt. Of these, three (the OBS site at 21°N on the East Pacific Rise, the Edmond site on the Central Indian Ridge, and the TAG site on the Mid-Atlantic Ridge) represent typical mid-ocean ridge basalt-hosted sites that are situated in an axial rift system—one on the valley floor (EPR 21°N), one on the rift valley wall (Edmond), and one on top of a rift-bounding fault

Table 4  
Summary of geologic settings and other general characteristics of the 12 hydrothermal vent sites considered in this study.

Vent site	Location	Depth (m)	Host rock	Setting	Hydrothermal venting
Rainbow	36°13'N 33°54'W	2300	Mantle peridotite with minor gabbroic rocks and basalt	South of Azores; in non-transform offset, bound to normal fault	Black smokers, $T < 365$ °C, pH ~ 3, little sediment
Logatchev	14°45'N 44°58'W	3000	Ultramafic/mafic, 20–40% gabbro intruded in residual mantle peridotite	South of 15°20'N Fracture Zone; in mega-breccia on a detachment fault	Black smokers, $T < 360$ °C, pH ~ 3, little sediment
Lost City	30°07'N 42°07'W	750	Mantle peridotite	At the summit of the Atlantis Massif; an outside corner high of the 30°N Fracture Zone	Clear fluids, $T > 110$ °C, pH ~ 11, carbonate-brucite chimneys, micritic carbonate sediment
Kairei	25°19'S 70°02'E	2450	Tholeiite/troctolite	North of Rodriguez Triple Junction (RTJ); on eastern shoulder of rift valley	Black smokers, $T < 360$ °C, pH ~ 3.5, little sediment, troctolite in recharge zone?
Edmond	23°52'S 69°35'E	3300	Tholeiite	At northern tip of the third ridge segment north of the RTJ, on western rift valley wall	Black smokers, $T < 382$ °C, pH ~ 3, little sediment, bacterial mats
Endeavour	47°57'N 129°05'W	2200	Tholeiite/sediment	Mid-segment of Endeavour Ridge; at base of western rift valley wall	Black smokers, $T < 375$ °C, pH ~ 4, sediment influence inferred from elevated CH <sub>4</sub> and NH <sub>4</sub> <sup>+</sup> of fluids
East Pacific Rise (EPR) 21°N	20°52'N 109°06'W	2600	Tholeiite	In small rift valley above eruptive fissures	Black smokers, $T < 350$ °C, pH ~ 3.5, little sediment
Lucky Strike	37°17'N 32°16'W	1700	Tholeiite/alkali basalt	South of Azores; At fringe of lava lake in summit caldera of a ridge centered seamount	Black smokers, $T < 328$ °C, pH ~ 4, little sediment
Trans-Atlantic Geotraverse (TAG)	26°08'N 44°49'W	3670	Tholeiite	On eastern shoulder of rift valley wall, bound to faults	Black smokers, $T < 365$ °C, pH ~ 4, large sulfide mound
Menez Gwen	37°50'N 31°31'W	850	Tholeiite/alkali basalt	South of Azores; in volcanic center in the central rift of a ridge centered seamount	Gray smokers, $T < 280$ °C, pH ~ 4.5, silica-barite slabs sealing seafloor
Brothers	34°51'S 179°03'E	1630	Calc-alkaline dacite to rhyodacite	In caldera of a submarine island arc volcano in the intraoceanic Kermadec arc	Black to gray smokers, $T < 290$ °C, pH ~ 2.8
Mariner	22°10'S 176°36'W	1910	Calc-alkaline basaltic andesite to andesite	From crest of Valu Fa Ridge in the Lau Basin; bound to fronts of lava flows and domes	Black to gray smokers, $T < 365$ °C, pH ~ 2.7

block (TAG) (Von Damm et al., 1985; Kleinrock and Humphris, 1996; Gallant and Von Damm, 2006). Similar rocks also host the fourth site, which is at the Endeavor hydrothermal field. However, the vent fluids there show clear evidence of contributions from buried sediments (Lilley et al., 1993). The last two sites—Lucky Strike and Menez Gwen south of the Azores platform—represent axial seamounts influenced by an area of enhanced melt production in the mantle (Parson et al., 2000). Both are developed in the summit areas of ridge-centered axial volcanoes and are tied to faults (bounding either a caldera or a graben), and both feature tholeiitic and alkaline basaltic lavas (Langmuir et al., 1997; Marques et al., 2009).

### 3.3. Felsic rock-hosted systems

Two sites (Brothers, Mariner) represent intraoceanic arc and associated backarc basin hydrothermal systems. The Brothers volcano in the Kermadec Arc is hosted in dacitic to rhyodacitic rocks (Haase et al., 2006), and fluids vent

in different areas within a central caldera and associated volcanic cone (de Ronde et al., 2005). Fluid compositions used in this study are from the NW caldera site (Takai et al., 2009). The Mariner hydrothermal field is located at the crest of the Valu Fa Ridge in the Lau Basin and features rocks of basaltic to andesitic compositions with clear island-arc affinity (Pearce et al., 1994; Bach et al., 1998). The vents are located in three clusters between the fronts of lava flows and lava domes. The fluid chosen for this study is from the Crab Restaurant area, where temperatures up to 279 °C were recorded (Takai et al., 2008).

### 3.4. Troctolite-basalt hybrid

The Kairei hydrothermal field, located on the shoulder of the Central Indian Ridge 22 km north of the Rodriguez Triple Junction, is hosted in normal mid-ocean ridge basalt, but it is apparently affected by another lithology. The elevated H<sub>2</sub> concentrations in the vent fluids (Gallant and Von Damm, 2006) can only be explained by interactions

with olivine-rich lithologies (Nakamura et al., 2009). Troctolites are abundant in outcrops surrounding the Kairei site, and it has been proposed that the circulating hydrothermal fluids encounter this olivine-plagioclase rock along their flow path (Nakamura et al., 2009).

## 4. RESULTS AND DISCUSSION

### 4.1. Catabolic reaction energetics

Reaction energetics for the seven net catabolic processes (Table 1) were evaluated for all 12 hydrothermal systems and plotted in Fig. 2 for two seawater:hydrothermal fluid (SW:HF) mixing ratios, representing 1% and 10% hydrothermal fluid in the binary mixtures. In the basalt-hosted and felsic rock-hosted systems, sulfide oxidation is clearly the dominant energy source at the low temperature scenario that corresponds to 1% HF input, accounting for up to ~95% of the available energy. In several of the hydrothermal systems, other reactions are also noteworthy and can yield moderate amounts of energy. For example, iron oxidation at Edmond and Mariner, hydrogen oxidation at EPR 21°N, and methane oxidation at Endeavor and Lucky Strike account for ~5–20% of the total. One outlier is Menez Gwen, where methane oxidation yields slightly more energy than sulfide oxidation at 1% HF input. Modeling results at 10% HF show that sulfide oxidation accounts for approximately half of the available energy, with the other half deriving from a combination of methane, iron, and/or hydrogen oxidation. See also in Fig. 2 that the anaerobic catabolisms (methanogenesis, sulfate reduction, AOM) are all energetically anemic at the basalt-hosted and felsic rock-hosted sites at both SW:HF ratios considered.

The peridotite-hosted systems, on the other hand, are characterized by a much larger diversity of catabolic energy sources and by relatively low energy yields from sulfide oxidation. At 1% HF, hydrogen oxidation dominates the energy landscape, with 38–56% of the total yield, but other aerobic reactions (methane oxidation, 20–28%; iron oxidation, up to ~19%) and anaerobic reactions (sulfate reduction, 6–9%; methanogenesis, 5–7%) also yield demonstrable energy. In the mixed solutions with 10% HF, up to six of the seven considered reactions yield almost identical energy. For example, at Rainbow, sulfate reduction, methanogenesis, and the oxidation of sulfide, methane, iron, or hydrogen each yields 13–20% of the total. Note also, that even AOM is minimally exergonic in the peridotite-hosted systems, both at 1% and 10% HF.

The troctolite-basalt hybrid at Kairei appears to be intermediate between the basalt-hosted and ferric rock-hosted systems on the one hand and the peridotite-hosted systems on the other. At both 1% and 10% HF, sulfide oxidation and hydrogen oxidation are the dominant chemolithotrophic energy sources, yielding 55–80% of the energy total. However, notable contributions also come from sulfate reduction (5–12%), methanogenesis (4–9%), and iron oxidation (7–17%).

To investigate the consequences of fluid composition over a much wider range of SW:HF ratios (and thus much broader temperature range), changes in reaction energetics

were evaluated for four hydrothermal systems, one example from each host rock type (Fig. 3). The total available energy in all four systems is greatest at low temperatures (and high SW:HF ratio), decreasing rapidly above ~10 °C. At Endeavor (basalt) and Mariner (felsic), the same catabolic processes (sulfide oxidation with lesser methane or iron oxidation) dominate over the entire temperature range investigated, yielding ~5.7 and ~7.5 kJ/kg vent fluid at low temperature and <~1 kJ/kg vent fluid above 25 °C from sulfide oxidation. At Rainbow (peridotite), however, a fundamental transformation in the energy landscape occurs with increasing temperature. Above ~45 °C, two anaerobic processes (sulfate reduction and methanogenesis) become more exergonic than their aerobic counterparts, despite the fact that oxidic seawater still accounts for >80% of the mixed solution at 45 °C. In fact, the energy yields from sulfate reduction and methanogenesis remain relatively constant (near 0.5 kJ/kg vent fluid) over the entire range of temperature and SW:HF mixing ratio investigated. At Kairei (troctolite-basalt), the energy yields from all aerobic and anaerobic reactions (except AOM) converge with increasing temperature, reaching a similar low value (~0.1–0.2 kJ/kg vent fluid) above ~80 °C.

The variability in geochemical energy sources among different vent systems (and at different temperatures within those systems), especially at the peridotite-hosted sites, may govern significant variations in metabolic and phylogenetic diversities of microbial communities that inhabit the different systems. Energy modeling can guide the exploration of these communities by predicting which catabolic strategies employed by archaeal and bacterial communities might dominate and which are likely to be rare. If catabolic energy availability dictates microbial community structure, mixing zones at Rainbow, for example, would be dominated by aerobes, especially hydrogen oxidizers, at low temperature sites, anaerobic sulfate reducers and methanogens at sites above ~60 °C, and evenly distributed numbers of aerobes and anaerobes at intermediate temperatures of ~35–50 °C. Note also that based on our thermodynamic modeling, net catabolic energy yields are highest at temperatures where psychrophiles (organisms with optimum growth temperatures <15 °C) dominate; energy yields at temperatures suitable for mesophiles and thermophiles (organisms that grow at moderate and elevated temperatures) are significantly lower. It should be kept in mind, however, that energy requirements for organisms at different temperatures may also differ significantly (McCollom and Amend, 2005; Amend and McCollom, 2009).

### 4.2. Anabolic reaction energetics

The focus is now shifted from catabolic to anabolic reaction energetics. The standard view of biological energy flow holds that catabolic processes drive the generation of ATP, which, when dephosphorylated, provides the energy needed to overcome thermodynamic barriers in anabolic processes. This, however, presupposes that all anabolic processes are endergonic, requiring external energy input to proceed. Our thermodynamic modeling demonstrates that under common geochemical conditions in deep-sea hydrothermal

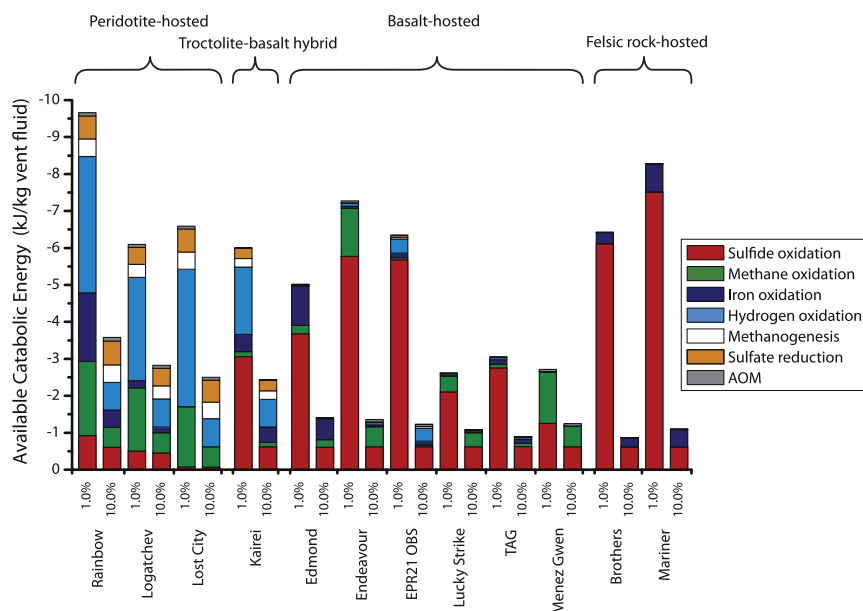


Fig. 2. Catabolic energies (in kJ per kg vent fluid) available from seven different redox reactions (see Table 1) in 12 hydrothermal systems hosted in peridotite, troctolite-basalt hybrid, basalt, and felsic rock. Values are computed at 1% and 10% hydrothermal fluid contribution to the mixed solutions.

systems, at least some biomass synthesis reactions can be accompanied by a net energy gain. Values of  $\Delta G_r$  for the synthesis of all the biomass monomers needed to construct a microbial cell are plotted in Fig. 4 for the most favorable temperatures (and batch mixing) conditions. Net anabolism at the peridotite-hosted sites (Rainbow, Logatchev, Lost City) and the troctolite-basalt hybrid (Kairei) are strongly exergonic, yielding approximately 700–870 J per g cell biomass. This energy yield may significantly reduce the total ATP requirement of growing cells or shunt the ‘extra’ ATP to drive thermodynamically unfavorable biomass synthesis, including polymerization reactions. At the basalt-hosted sites, however, the energetics of anabolism are much less favorable, ranging from a moderately exergonic  $-400$  J at Endeavour to a moderately endergonic  $+250$  J at Menez Gwen per g cell biomass synthesized. On average, the synthesis of all biomonomers needed for cell construction hovers near equilibrium ( $\Delta G = 0$ ) at the geochemically optimal conditions in basalt hydrothermal systems. Lastly, net anabolism is also endergonic at felsic rock-hosted Brothers and Mariner, requiring  $\sim 135$ – $270$  J per g dry cell mass.

Reaction energetics for biomass synthesis were also evaluated as a function of temperature (and SW:HF ratio) in four hydrothermal systems, one from each host rock type (Fig. 5). It can be seen that the energetics for total cell synthesis (black curves in Fig. 5) are exergonic at Rainbow (peridotite) and Kairei (troctolite-basalt), but endergonic at Mariner (felsic) over the entire temperature range investigated; at Endeavour (basalt), total cell biomass synthesis is exergonic below  $\sim 90$  °C, and endergonic at higher temperature. The energy contributions from each family of monomer compounds (amino acids, nucleotides, fatty acids, saccharides, and amines) are positive for some, but negative

for others, and values of  $\Delta G_r$  differ substantially from site to site. However, for all monomer families (and for total cell),  $\Delta G_r$  decreases dramatically with increasing temperature from 2 °C (100% seawater), minimizing near 30 °C, before gradually increasing with increasing temperature and hydrothermal fluid contribution. In addition, the relative positions of the colored curves in Fig. 5 (representing the energetics of the different monomer families) are also similar among the four model systems. The synthesis of amino acids and fatty acids are, with one exception (amino acids at Mariner above  $\sim 55$  °C), thermodynamically the most favorable, followed by the synthesis of saccharides and amines, which are energetically nearly identical; the synthesis of nucleotides is thermodynamically the least favorable at each site and mixing regime. A focused analysis of Fig. 5 further reveals that the anabolic energy landscapes at Rainbow and Kairei are nearly identical—amino acid and fatty acid synthesis are both exergonic over the entire temperature range, with values of  $\Delta G$  down to approximately  $-700$  J and  $-300$  J per g of cell biomass, respectively; the synthesis of saccharides and amines is near equilibrium ( $\Delta G = 0$ ) at all temperatures and SW:HF ratios considered, and that of nucleotides is endergonic, consuming a minimum of  $\sim 250$  J per g. The energy landscape at Endeavour is qualitatively similar to those at Rainbow and Kairei, but the synthesis of amino acids and fatty acids is less favorable, with values of  $\Delta G$  minimizing near  $-450$  and  $-200$  J/g, respectively. Mariner is energetically the least favorable, with the synthesis of fatty acids and amino acids (at  $\sim 5$ – $55$  °C) only slightly exergonic, and that of nucleotides the most endergonic of all the anabolic processes considered.

Close scrutiny of the reaction energetics for both catabolic and anabolic processes underscores a clear

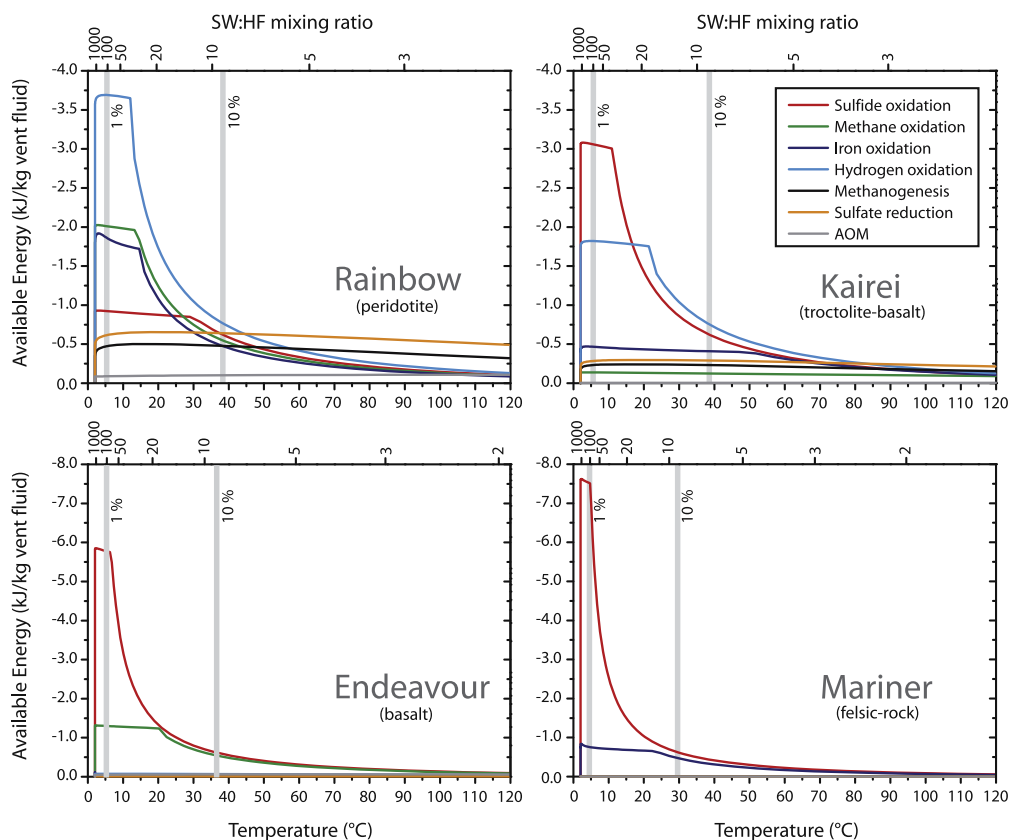


Fig. 3. Catabolic energies (in kJ per kg vent fluid) available from seven different redox reactions (see Table 1) as a function of temperature and seawater:hydrothermal fluid (SW:HF) mixing ratio in four different vent systems. The 1% and 10% hydrothermal fluid contribution to the mixed solutions are indicated for context. Owing to different vent fluid temperatures, the scales for the SW:HF mixing ratio are slightly different in the four panels.

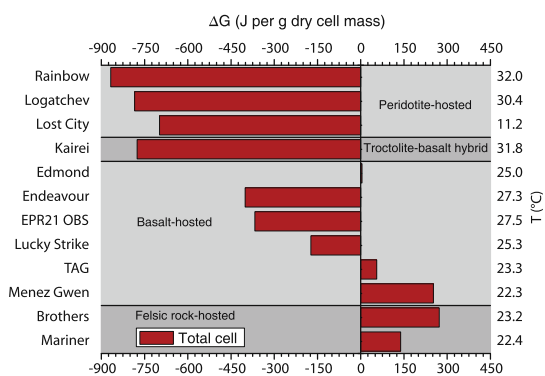


Fig. 4. Gibbs energies (in J per g dry cell mass) of the sum total of the anabolic reactions in the 12 hydrothermal systems calculated at the energetically most favorable SW:HF mixing ratio (between 5.8% and 8.3% hydrothermal fluid). The temperatures to which these ratios correspond are given on the right hand side.

biogeochemical distinction between peridotite-hosted (and perhaps troctolite-basalt hybrid) systems on the one hand and basalt-hosted (and perhaps felsic rock-hosted) systems on the other. In catabolic reactions, this split is manifested

by a difference in the most exergonic reactions—hydrogen oxidation in peridotite and sulfide oxidation in basalt. In anabolic reactions, it is manifested in the amount of energy released or consumed—total cell biomass synthesis is strongly exergonic in peridotite, but only moderately exergonic to moderately endergonic in basalt. An integration of all the results points to hydrogen concentration as arguably the most influential geochemical factor determining the sum of anabolic and catabolic reaction energetics in the wide spectrum of submarine hydrothermal systems. Differences in vent fluid temperature (140–382 °C), pH (1.2–9), CO<sub>2</sub> (0.01–93.3 mM), and H<sub>2</sub>S (0.01 μM to 7.4 mM), for example, dictate the energetics of biomass synthesis far less than do the differences in H<sub>2</sub> (0.02–16 mM). Effects on the energetics of net catabolisms are often dominated by hydrogen concentration, but in some cases (e.g., basalt-hosted systems) sulfide concentration may play at least an equally important role. The overall dominant role of H<sub>2</sub> in the reaction energetics is also a function of the reaction stoichiometries in anabolism and catabolism, where the stoichiometric reaction coefficient for H<sub>2</sub> is usually greater than that for the other species involved (see Tables 1 and 2). Note, even at the highest temperatures considered (120 °C), the chemistries of the mixed solutions are

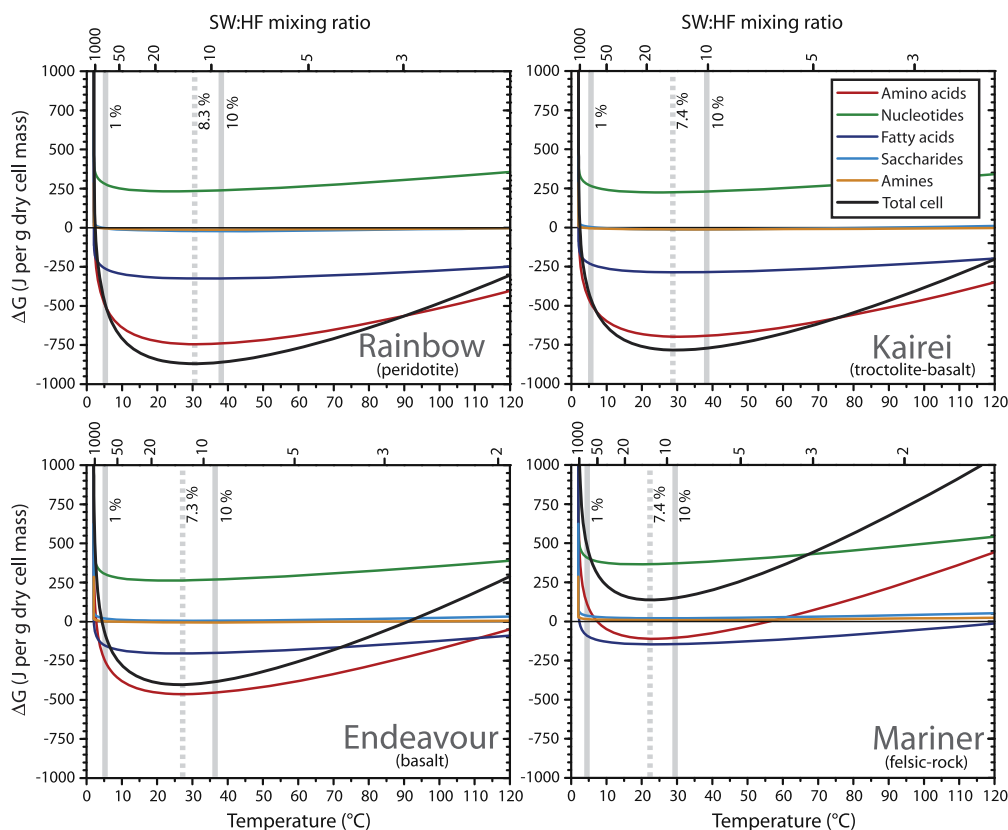


Fig. 5. Gibbs energies (in J per g dry cell mass) of anabolic reactions as a function of temperature and SW:HF mixing ratio in four different vent systems. Curves represent individual monomer families (e.g., amino acids, and nucleotides) and the sum total for cell biomass. Owing to different vent fluid temperatures, the scales for the SW:HF mixing ratio are slightly different in the four panels.

dominated by oxic seawater, but interestingly, in the peridotite-hosted and troctolite-basalt systems, the most exergonic chemolithotrophic reactions shift from aerobic respiration (oxidation of hydrogen, sulfide, iron, and methane) at lower temperatures to anaerobic respiration (sulfate reduction and methanogenesis) at higher temperatures. Numerical models that consider diffusion and advection in addition to fluid mixing indicate that such factors have little impact on the overall energetics of metabolic reactions, although they may shift the temperature range over which aerobic catabolisms are favorable to higher or lower temperatures (Tivey, 2004).

## 5. CONCLUDING REMARKS

In our modeling approach, the catabolic and anabolic reactions are competing for many of the same reactants, and thus the reported energy yields cannot be achieved simultaneously. A fully coupled reaction-transport model that could shine light on this issue is beyond the scope of this study. Note however, that in dynamic hydrothermal systems, the transport of aqueous species by diffusion and/or advection is rapid, and essential nutrients required by active microbial communities will be replenished perhaps within hours (Tivey, 1995, 2004). The combination of catabolic and anabolic reaction energetics evaluated here

for a range of geochemical conditions can generate testable models of archaeal and bacterial metabolic strategies in deep-sea hydrothermal systems. We recognize that other factors, including convective heat transport, phase separation, residence time, and microbial metabolisms, can cause fluid composition versus temperature trends to deviate somewhat from those represented by our calculations, but we maintain that the host rock and fluid-rock interactions are the most influential drivers of fluid chemistry. The approach outlined and adopted here is highly relevant to vent plumes and seafloor and shallow-subseafloor sites in deep-sea hydrothermal systems, but it can also be applied to shallow-sea and continental hydrothermal systems, or to any system where fluids of different compositions mix to generate redox disequilibria.

## ACKNOWLEDGMENTS

This research was supported by an NSF-RIDGE Grants 0937337 (to J.P.A.) and 0937309 (to T.M.M.). We thank Niels Jöns for generating Fig. 1.

## REFERENCES

Amend J. P. and McCollom T. M. (2009) Energetics of biomolecule synthesis on early Earth. In *Chemical Evolution II: From*

- the Origins of Life to Modern Society, Vol. 1025* (eds. L. Zaikowski, J. M. Friedrich and S. R. Seidel). American Chemical Society (pp. 63–94).
- Amend J. P. and Plyasunov A. V. (2001) Carbohydrates in thermophile metabolism: Calculation of the standard molal thermodynamic properties of aqueous pentoses and hexoses at elevated temperatures and pressures. *Geochimica et Cosmochimica Acta* **65**, 3901–3917.
- Amend J. P. and Shock E. L. (1998) Energetics of amino acid synthesis in hydrothermal ecosystems. *Science* **281**, 1659–1662.
- Bach W., Banerjee N. R., Dick H. J. B. and Baker E. T. (2002) Discovery of ancient and active hydrothermal systems along the ultra-slow spreading Southwest Indian Ridge 10–16 E. *Geochemistry, Geophysics, Geosystems* **3**. doi:10.1029/2001GC000279.
- Bach W., Hegner E. and Erzinger J. (1998) Chemical fluxes in the Tonga subduction zone: evidence from the southern Lau Basin. *Geophysical Research Letters* **25**, 1467–1470.
- Baross J. A. and Hoffman S. E. (1985) Submarine hydrothermal vents and associated gradient environments as sites for the origin and evolution of life. *Origins of Life* **15**, 327–345.
- Battley E. H. (1991) An alternate method of calculating the heat of growth of *Escherichia coli* K-12 on succinic acid. *Biotechnology and Bioengineering* **38**, 480–492.
- Biddle J. F., Fitz-Gibbon S., Schuster S. C., Brenchley J. E. and House C. H. (2008) Metagenomic signatures of the Peru Margin seafloor biosphere show a genetically distinct environment. *Proceedings of the National Academy of Sciences, USA* **105**, 10583–10588.
- Boschi C., Früh-Green G. L., Delacour A., Karson J. A. and Kelley D. S. (2006) Mass transfer and fluid flow during detachment faulting and development of an oceanic core complex, Atlantis Massif (MAR 30 N). *Geochemistry, Geophysics, Geosystems* **7**. doi:10.1029/2005GC001074.
- Charlou J. L., Donval J., Jean-Baptiste P., Dapigny A. and Rona P. (1996) Gases and helium isotopes in high temperature solutions sampled before and after ODP Leg 158 drilling at TAG hydrothermal field (26 N, MAR): TAG. *Geophysical Research Letters* **23**, 3491–3494.
- Charlou J. L., Donval J. P., Douville D., Knoery J., Fouquet Y., Jean-Baptiste P., Bourg C., Prieur D. and German C. (1998) Fluides hydrothermaux en contexte de roches ultrabasiqes: exemples de Logatchev (14j45VN) et Rainbow (36j14VN) sur la dorsale médio-Atlantique. *Réunion des Sciences de la Terre RST* **31**(98), 89.
- Charlou J. L., Donval J. P., Douville E., Jean-Baptiste P., Radford-Knoery J., Fouquet Y., Dapigny A. and Stievenard M. (2000) Compared geochemical signatures and the evolution of Menez Gwen (37 50'N) and Lucky Strike (37 17'N) hydrothermal fluids, south of the Azores Triple Junction on the Mid-Atlantic Ridge. *Chemical Geology* **171**, 49–75.
- Charlou J. L., Donval J. P., Fouquet Y., Jean-Baptiste P. and Holm N. G. (2002) Geochemistry of high H<sub>2</sub> and CH<sub>4</sub> vent fluids issuing from ultramafic rocks at the Rainbow hydrothermal field (36 14'N, MAR). *Chemical Geology* **191**, 345–359.
- D'Hondt S., Jørgensen B. B., Miller D. J., Batzke A., Blake R., Cragg B. A., Cypionka H., Dickens G. R., Ferdelman T., Hinrichs K.-U., Holm N. G., Mitterer R., Spivack A., Wang G., Bekins B., Engelen B., Ford K., Gettemy G., Rutherford S. D., Sass H., Skilbeck C. G., Aiello I. W., Guerin G., House C. H., Inagaki F., Meister P., Naehr T., Niitsuma S., Parkes R. J., Schippers A., Smith D. C., Teske A., Wiegand J., Padilla C. N. and Acosta J. L. S. (2004) Distribution of microbial activities in deep seafloor sediments. *Science* **306**, 2216–2221.
- D'Hondt S., Spivack A. J., Pockalny R., Ferdelman T. G., Fischer J. P., Kallmeyer J., Abrams L. J., Smith D. C., Graham D., Hasiuk, Schrum H. and Stancin A. M. (2009) Subseafloor sedimentary life in the South Pacific Gyre. *Proceedings of the National Academy of Sciences, USA* **106**, 11651–11656.
- de Ronde C. E. J., Hannington M. D., Stoffers P., Wright I., Ditchburn R. G., Reyes A. G., Baker E. T., Massoth G., Lupton J., Walkers S. L., Greene R. R., Soong C. W. R., Ishibashi J., Lebon G., Bray C. J. and Resing J. A. (2005) Evolution of a submarine magmatic-hydrothermal system: Brothers volcano, southern Kermadec Arc, New Zealand. *Economic Geology* **100**, 1097–1133.
- Delacour A., Früh-Green G. L., Bernasconi S. M., Schaeffer P. and Kelley D. S. (2008) Carbon geochemistry of serpentinites in the Lost City Hydrothermal System (30 N, MAR). *Geochimica Cosmochimica Acta* **72**, 3681–3702.
- Dick J. M., LaRowe D. E. and Helgeson H. C. (2006) Temperature, pressure, and electrochemical constraints on protein speciation: group additivity calculation of the standard molal thermodynamic properties of ionized unfolded proteins. *Bio-geosciences* **3**, 311–336.
- Douville E., Charlou J. L., Oelkers E. H., Bienvenu P., Jove Colon C. F., Donval J. P., Fouquet Y., Prieur D. and Appriou P. (2002) The Rainbow vent fluids (36 14'N, MAR): the influence of ultramafic rocks and phase separation on trace metal content in Mid-Atlantic hydrothermal fluids. *Chemical Geology* **184**, 37–48.
- Drummond S. E. J. (1981) Boiling and mixing of hydrothermal fluids: Chemical effects on mineral precipitation. Ph. D. thesis, Pennsylvania State University.
- Foustoukos D. I. and Seyfried W. E. (2004) Hydrobarbons in hydrothermal vent fluids: the role of chromium-bearing catalysts. *Science* **304**, 1002–1005.
- Früh-Green G. L., Connolly J. A. D., Plas A., Kelley D. S. and Grobety B. (2004) Serpentinization of ocean peridotites: implications for geochemical cycles and biological activity. In *The Subseafloor Biosphere at Mid-Ocean Ridges, Vol. 144* (eds. W. S. D. Wilcock, E. F. DeLong, D. S. Kelley, J. A. Baross and S. C. Cary). American Geophysical Union (pp. 119–136).
- Früh-Green G. L., Kelley D. S., Bernasconi S. M., Karson J. A., Ludwig K. A., Butterfield D. A., Boschi C. and Proskurowski G. (2003) 30,000 years of hydrothermal activity at the Lost City vent field. *Science* **30**, 495–498.
- Gallant R. M. and Von Damm K. L. (2006) Geochemical controls on hydrothermal fluids from the Kairei and Edmond Vent Fields, 23–25 S, Central Indian Ridge. *Geochemistry, Geophysics, Geosystems* **7**, 1–24.
- German C. R. and Parson L. M. (1998) Distributions of hydrothermal activity along the Mid-Atlantic Ridge: interplay of magmatic and tectonic control. *Earth and Planetary Science Letters* **160**, 327–341.
- Haase K. M., Stroncik N. A., Garbe-Schönberg D. and Stoffers P. (2006) Formation of island arc dacite magmas by extreme crystal fractionation: An example from Brothers Seamount, Kermadec Island arc (SW Pacific). *Journal of Volcanology and Geothermal Research* **152**, 316–330.
- Hannington M. D., de Ronde C. E. J. and Petersen S. (2005) Seafloor tectonics and submarine hydrothermal systems. *Economic Geology* **100**, 111–143.
- Helgeson H. C., Delany J. M., Nesbitt W. H. and Bird D. K. (1978) Summary and critique of the thermodynamic properties of rock-forming minerals. *American Journal of Science* **278A**, 1–229.
- Helgeson H. C., Kirkham D. H. and Flowers G. C. (1981) Theoretical prediction of the thermodynamic behavior of aqueous electrolytes at high pressures and temperatures: IV. Calculation of activity coefficients, osmotic coefficients, and apparent molal and standard and relative partial molal prop-

- erties to 600 °C and 5 kb. *American Journal of Science* **281**, 1249–1516.
- Jahnke R. A. (1996) The global ocean flux of particulate organic carbon: Areal distribution and magnitude. *Global Biogeochemical Cycles* **10**, 71–88.
- Johnson J. W., Oelkers E. H. and Helgeson H. C. (1992) SUPCRT92: a software package for calculating the standard molal properties of minerals, gases, aqueous species, and reactions from 1 to 5000 bar and 0 to 1000 °C. *Computers and Geosciences* **18**(7), 899–947.
- Jørgensen B. B. and D'Hondt S. (2006) A starving majority deep beneath the seafloor. *Science* **314**, 932–934.
- Kelley D. S. and Früh-Green G. L. (2001) Volatile lines of descent in submarine plutonic environments: insights from stable isotope and fluid inclusion analyses. *Geochimica Cosmochimica Acta* **65**, 3325–3346.
- Kelley D. S., Karson J. A., Blackman D. K., Früh-Green G. L., Butterfield D. A., Lilley M. D., Olson E. J., Schrenk M. O., Roe K. K., Lebon G. T., Rivizzigno P. and Party A.-S. (2001) An off-axis hydrothermal vent field near the Mid-Atlantic Ridge at 30 N. *Nature* **412**, 145–149.
- Kelley D. S., Karson J. A., Früh-Green G. L., Yoerger D. R., Shank T. M., Butterfield D. A., Hayes J. M., Schrenk M. O., Olson E. J., Proskurowski G., Jakuba M., Bradley A., Larson B., Ludwig K., Glickson D., Buckman K., Bradley A. S., Brazelton W. J., Roe K., Elend M. J., Delacour A., Bernasconi S. M., Lilley M. D., Baross J. A., Summons R. E. and Sylva S. P. (2005) A serpentinite-hosted ecosystem: the Lost City hydrothermal field. *Science* **307**, 1428–1434.
- Kleinrock M. C. and Humphris S. E. (1996) Structural controls on the localization of seafloor hydrothermal activity at the TAG active mound, Mid-Atlantic Ridge. *Nature* **382**, 149–153.
- Konn C., Charlou J. L., Donval J. P., Holm N. G., Dehairs F. and Bouillon S. (2009) Hydrocarbons and oxidized organic compounds in hydrothermal fluids from Rainbow and Lost City ultramafic hosted vents. *Chemical Geology* **258**, 299–314.
- Lang S. Q., Butterfield D., Schulte M., Kelley D. S. and Lilley M. D. (2010) Elevated concentrations of formate, acetate and dissolved organic carbon found at the Lost City hydrothermal field. *Geochimica Cosmochimica Acta* **74**, 941–952.
- Langmuir C., Humphris S., Fornari D., Van Dover C., Von Damm K., Tivey M. K., Colodner D., Charlou J.-L., Desonie D., Wilson C., Fouquet Y., Klinkhammer G. and Bougault H. (1997) Hydrothermal vents near a mantle hot spot: the Lucky Strike vent field at 37 N on the Mid-Atlantic Ridge. *Earth and Planetary Science Letters* **148**, 69–91.
- LaRowe D. E. and Helgeson H. C. (2006) Biomolecules in hydrothermal systems: calculation of the standard molal thermodynamic properties of nucleic-acid bases, nucleosides, and nucleotides at elevated temperatures and pressures. *Geochimica Cosmochimica Acta* **70**, 4680–4724.
- LaRowe D. E. and Regnier P. (2008) Thermodynamic potential for the abiotic synthesis of adenine, cytosine, guanine, thymine, uracil, ribose, and deoxyribose in hydrothermal systems. *Origins of Life and Evolution of the Biosphere* **38**, 383–397.
- Lilley M. D., Butterfield D. A., Lupton J. E. and Olson E. J. (2003) Magmatic events can produce rapid changes in hydrothermal vent chemistry. *Nature* **422**, 878–881.
- Lilley M. D., Butterfield D. A., Olson E. J., Lupton J. E., Macko S. A. and McDuff R. E. (1993) Anomalous CH<sub>4</sub> and NH<sub>4</sub><sup>+</sup> concentrations at an unsedimented mid-ocean ridge hydrothermal system. *Nature* **364**, 45–47.
- Marques A. F. A., Barriga F., Chavagnac V. and Fouquet Y. (2006) Mineralogy, geochemistry, and Nd isotope composition of the Rainbow hydrothermal field, Mid-Atlantic Ridge. *Mineralium Deposita* **41**, 52–67.
- Marques A. F. A., Scott S. D., Gorton M. P., Barriga F. J. A. S. and Fouquet Y. (2009) Pre-eruption history of enriched MORB from the Menez Gwen (37°50'N) and Lucky Strike (37°17'N) hydrothermal systems, Mid-Atlantic Ridge. *Lithos* **112**, 18–39.
- Martin W., Baross J. A., Kelley D. S. and Russell M. J. (2008) Hydrothermal vents and the origin of life. *Nature* **6**, 805–814.
- McCollom T. M. (2000) Geochemical constraints on primary productivity in submarine hydrothermal vent plumes. *Deep-Sea Research I* **47**, 85–101.
- McCollom T. M. (2007) Geochemical constraints on sources of metabolic energy for chemolithoautotrophy in ultramafic-hosted deep-sea hydrothermal systems. *Astrobiology* **7**, 933–950.
- McCollom T. M. and Amend J. P. (2005) A thermodynamic assessment of energy requirements for biomass synthesis by chemolithoautotrophic micro-organisms in oxic and anoxic environments. *Geobiology* **3**, 135–144.
- McCollom T. M. and Shock E. L. (1997) Geochemical constraints on chemolithoautotrophic metabolism by microorganisms in seafloor hydrothermal systems. *Geochimica et Cosmochimica Acta* **61**, 4375–4391.
- Morowitz H. J. (1968) *Energy Flow in Biology*. Academic Press.
- Nakamura K., Morishita T., Bach W., Klein F., Hara K., Okino K., Takai K. and Kumagai H. (2009) Serpentinized troctolites exposed near the Kairei Hydrothermal Field, Central Indian Ridge: Insights into the origin of the Kairei hydrothermal fluid supporting a unique microbial ecosystem. *Earth and Planetary Science Letters* **280**, 128–136.
- Pace N. R. (1991) Origin of life: facing up to the physical setting. *Cell* **65**, 531–533.
- Parkes R. J., Cragg B. A. and Wellsbury P. (2000) Recent studies on bacterial populations and processes in subseafloor sediments: a review. *Hydrogeology Journal* **8**, 11–28.
- Parson L., Gracia E., Collier D., German C. and Needham D. (2000) Second-order segmentation; the relationship between volcanism and tectonism at the MAR, 38°N–35°40'PN. *Earth and Planetary Science Letters* **178**, 231–251.
- Pearce P. A., Ernewein M., Bloomer S. H., Parson L. M., Murton B. J. and Johnson L. E. (1994) Geochemistry of Lau Basin volcanic rocks: influence of ridge segmentation and arc proximity. In *Volcanism Associated With Extension at Consuming Plate Margins* (ed. J. L. Smellie). Geological Society of America.
- Petersen S., Kuhn K., Kuhn T., Augustin N., Hekinian R., Franz L. and Borowski C. (2009) The geological setting of the ultramafic-hosted Logatchev hydrothermal field (14°45'N, Mid-Atlantic Ridge) and its influence on massive sulfide formation. *Lithos* **112**, 40–56.
- Proskurowski G., Lilley M. D., Kelley D. S. and Olson E. J. (2006) Low temperature volatile production at the Lost City Hydrothermal Field, evidence from a hydrogen stable isotope geothermometer. *Chemical Geology* **229**, 331–343.
- Proskurowski G., Lilley M. D., Seewald J. S., Früh-Green G. L., Olson E. J., Lupton J. E., Sylva S. P. and Kelley D. S. (2008) Abiogenic hydrocarbon production at Lost City hydrothermal field. *Science* **319**, 604–607.
- Roussel E. G., Bonavita M. A., Querellou J., Cragg B. A., Wester G., Prieur D. and Parkes R. J. (2008) Extending the sub-seafloor biosphere. *Science* **320**, 1046.
- Russell M. J. and Hall A. J. (1997) The emergence of life from iron monosulphide bubbles at a submarine hydrothermal redox and pH front. *Journal of the Geological Society, London* **154**, 377–402.
- Russell M. J., Hall A. J., Boyce A. J. and Fallick A. E. (2005) On hydrothermal convection systems and the emergence of life. *Economic Geology* **100**, 419–438.

- Schmidt K., Koschinsky A., Garbe-Schönberg D., de Carvalho L. M. and Seifert R. (2007) Geochemistry of hydrothermal fluids from the ultramafic-hosted Logatchev hydrothermal field, 15 N on the Mid-Atlantic Ridge: Temporal and spatial investigation. *Chemical Geology* **242**, 1–21.
- Schroeder T., Cheadle M. J., Dick H. J. B., Faul U., Casey J. F. and Keleman P. B. (2007) Nonvolcanic seafloor spreading and corner-flow rotation accommodated by extensional faulting at 15 N on the Mid-Atlantic Ridge: a structural synthesis of ODP Leg 209. *Geochemistry, Geophysics, Geosystems* **8**. doi:10.1029/2006GC001567.
- Seewald J. S., Cruse A. and Saccoccia P. (2003) Aqueous volatiles in hydrothermal fluids from the Main Endeavour Field, northern Juan de Fuca Ridge: temporal variability following earthquake activity. *Earth and Planetary Science Letters* **216**, 575–590.
- Seyfried W. E., Seewald J. S., Berndt M. E., Ding K. and Foustoukos D. I. (2003) Chemistry of hydrothermal vent fluids from the Main Endeavour Field, northern Juan de Fuca Ridge: Geochemical controls in the aftermath of June 1999 seismic events. *Journal of Geophysical Research* **108**. doi:10.1029/2002JB001957.
- Shock E. and Canovas P. (2010) The potential for abiotic organic synthesis and biosynthesis at seafloor hydrothermal systems. *Geofluids* **10**, 161–192.
- Shock E. L., Amend J. P. and Zolotov M. Y. (2000) The early Earth vs. the origin of life. In *Origin of the Earth, Moon* (eds. R. Canup and K. Righter). The University of Arizona Press (pp. 527–543).
- Shock E. L. and Helgeson H. C. (1988) Calculation of the thermodynamic and transport properties of aqueous species at high pressures and temperatures: Correlation algorithms for ionic species and equation of state predictions to 5 kb and 1000 °C. *Geochimica et Cosmochimica Acta* **52**, 2009–2036.
- Shock E. L. and Helgeson H. C. (1990) Calculation of the thermodynamic and transport properties of aqueous species at high pressures and temperatures: standard partial molal properties of organic species. *Geochimica et Cosmochimica Acta* **54**, 915–945.
- Shock E. L., Helgeson H. C. and Sverjensky D. A. (1989) Calculation of the thermodynamic and transport properties of aqueous species at high pressures and temperatures: standard partial molal properties of inorganic neutral species. *Geochimica et Cosmochimica Acta* **53**(9), 2157–2183.
- Shock E. L. and Holland M. E. (2004) Geochemical energy sources that support the subsurface biosphere. In *The Subseafloor Biosphere at Mid-Ocean Ridges, Geophysical Monograph, Vol. 144* (eds. W. S. D. Wilcock, E. F. DeLong, D. S. Kelley, J. A. Baross and S. C. Cary). American Geophysical Union (pp. 153–165).
- Shock E. L., Oelkers E. H., Johnson J. W., Sverjensky D. A. and Helgeson H. C. (1992) Calculation of the thermodynamic properties of aqueous species at high pressures and temperatures: effective electrostatic radii, dissociation constants and standard partial molal properties to 1000 °C and 5 kbar. *Journal of the Chemical Society Faraday Transactions* **88**(6), 803–826.
- Shock E. L. and Schulte M. D. (1998) Organic synthesis during fluid mixing in hydrothermal systems. *Journal of Geophysical Research* **103**, 28513–28527.
- Takai K. and Nakamura K. (2010) Compositional, physiological and metabolic variability in microbial communities associated with geochemically diverse, deep-sea hydrothermal vent fluids. In *Geomicrobiology: Molecular, Environmental Perspective* (eds. L. Barton, M. Mendl and A. Loy). Springer (pp. 251–283).
- Takai K., Nunoura T., Horikoshi K., Shibuya T., Nakamura K., Suzuki Y., Stott M., Massoth G. J., Christenson B. W., deRonde C. E. J., Butterfield D. A., Ishibashi J., Lupton J. E. and Evans L. J. (2009) Variability in microbial communities in black smoker chimneys at the NW Caldera Vent Field, Brothers Volcano, Kermadec Arc. *Geomicrobiology Journal* **26**, 552–569.
- Takai K., Nunoura T., Ishibashi J., Lupton J. E., Suzuki R., Hamasaki H., Ueno Y., Kawagucci S., Gamo T., Suzuki Y., Hirayama H. and Horikoshi K. (2008) Variability in the microbial communities and hydrothermal fluid chemistry at the newly discovered Mariner hydrothermal field, southern Lau Basin. *Journal of Geophysical Research* **113**.
- Tanger J. C. and Helgeson H. C. (1988) Calculation of the thermodynamic and transport properties of aqueous species at high pressures and temperatures: revised equations of state for the standard partial molal properties of ions and electrolytes. *American Journal of Science* **288**, 19–98.
- Tivey M. K. (1995) The influence of hydrothermal fluid composition and advection rates on black smoker mineralogy and texture: insights from modeling transport and reaction. *Geochimica et Cosmochimica Acta* **59**, 1933–1949.
- Tivey M. K. (2004) Environmental conditions within active seafloor vent structures: sensitivity to vent fluid composition and fluid flow. In *Subseafloor Biosphere at Mid-Ocean Ridges, Vol. 144* (eds. W. S. D. Wilcock, E. F. DeLong, D. S. Kelley, J. A. Baross and S. C. Cary). American Geophysical Union (pp. 137–152).
- Von Damm K. L. (1990) Seafloor hydrothermal activity: black smoker chemistry and chimneys. *Annual Reviews in Earth and Planetary Science* **18**, 173–204.
- Von Damm K. L., Edmond J. M., Grant B., Measures C. I., Walden B. and Weiss R. F. (1985) Chemistry of submarine hydrothermal solutions at 21 N, East Pacific Rise. *Geochimica et Cosmochimica Acta* **49**, 2197–2220.
- Webster G., Blazejak A., Cragg B. A., Schippers A., Sass H., Rinna J., Tang X., Mathes F., Ferdelman T. G., Fry J. C., Weightman A. J. and Parkes R. J. (2009) Subsurface microbiology and biogeochemistry of a deep, cold-water carbonate mound from the Porcupine Seabight (IODP Expedition 307). *Environmental Microbiology* **11**, 239–257.
- Welhan J. A. and Craig H. (1983) Methane, hydrogen, and helium in hydrothermal fluids at 21 N on the East Pacific Rise. In *Hydrothermal Processes at Seafloor Spreading Centers* (ed. P. A. E. A. Rona). Plenum (pp. 391–409).
- Wolery T. J. (2004) *Qualification of thermodynamic data for geochemical modeling of mineral–water interactions in dilute systems*. US Department of Energy, Bechtel SAIC Company, LLC.

Associate editor: Johnson R. Haas